Research Square

Preprints are preliminary reports that have not undergone peer review.
They should not be considered conclusive, used to inform clinical practice,
or referenced by the media as validated information.

CoPeX: A Novel Complex-Domain SSA–FTBPF Method for Polar Motion Periodic Component Extraction

Qi Bai
Wuhan University
Jian Wang
Wuhan University
Kehao Yu
kehaoyu@whu.edu.cn
Wuhan University

Research Article

Keywords: polar motion, Chandler wobble, annual wobble, singular spectrum analysis, Fourier transform band pass filtering

Posted Date: November 25th, 2026

DOI: https://doi.org/10.21203/rs.3.rs-11622920/v1

License: This work is licensed under a Creative Commons Attribution 4.0 International License.
Read Full License

Additional Declarations: No competing interests reported.

CoPeX: A Novel Complex-Domain SSA–FTBPF Method for Polar Motion Periodic Component Extraction

Qi Bai[1], Jian Wang[2], Kehao Yu[1,2]

1 School of Geodesy and Geomatics, Wuhan University, Wuhan 430079, China

2 GNSS Research Center, Wuhan University, Wuhan 430079, China

Corresponding Author:

Kehao Yu, ✉ kehaoyu@whu.edu.cn

Abstract

The Chandler wobble (CW) and annual wobble (AW) are the two principal oscillatory components of polar motion (PM). Their closely spaced frequencies, together with temporal variations in amplitude and phase, pose challenges to their accurate separation. Singular spectrum analysis (SSA) is susceptible to mode mixing when decomposing quasi-periodic signals, whereas Fourier transform band pass filtering (FTBPF) is sensitive to residual trends and boundary effects. To address these limitations, we propose a complex-domain method, termed CoPeX, that integrates SSA and FTBPF to extract CW and AW. CoPeX combines PMX and PMY into a complex-valued series, uses SSA to derive preliminary CW and AW components, and subsequently refines them through FTBPF. Simulation results show that CoPeX reduces the root-mean-square errors (RMSEs) of CW and AW by 29.30% and 3.84%, respectively, compared with SSA, and by 63.20% and 22.76%, respectively, compared with FTBPF. Application to the International Earth Rotation and Reference Systems Service (IERS) C04 PM series reveals that CoPeX produces more concentrated spectral energy than either SSA or FTBPF, effectively mitigating cross-contamination between CW and AW and enabling more reliable estimation of their time-varying amplitudes and phases.

Keywords: polar motion; Chandler wobble; annual wobble; singular spectrum analysis; Fourier transform band pass filtering

1 Introduction

Polar motion (PM), one of the fundamental Earth orientation parameters (EOP), describes the motion of the Celestial Intermediate Pole (CIP) in the terrestrial reference frame and is commonly represented by two orthogonal components, PMX and PMY (Bizouard et al. 2019; Rekier et al. 2022; Li et al. 2026). The low-frequency variability of PM is mainly characterized by two narrow-band oscillations, namely the Chandler wobble (CW) near 0.84 cycles per year and the annual wobble (AW) at 1 cycle per year (Höpfner 2004; Yu et al. 2025). The CW is the Earth's free rotational mode, whose eigenfrequency is governed primarily by the Earth's equatorial ellipticity, elastic

response, and internal structure, whereas its amplitude and phase vary in response to geophysical excitations (Wang et al. 2016; Chen et al. 2023; Jeon et al. 2025; Shi et al. 2025). In contrast, the AW is a forced seasonal oscillation driven mainly by the annual redistribution of mass and angular momentum in the atmosphere, oceans, continental hydrosphere, and cryosphere (Dickey et al. 1993; Wang et al. 2025a, b). The CW and AW are therefore not merely periodic components of PM, but observed rotational signals associated with mass redistribution and angular-momentum exchange within the Earth system. Their temporal variations are closely related to climate-driven surface mass changes, hydrological and cryospheric processes, and anomalous variations in Earth rotation (Kiani Shahvandi et al. 2024). However, the proximity of the Chandler and annual frequencies, together with the time-dependent amplitudes and phases of the two components, makes their separation from PM time series challenging (Schuh et al. 2001). Reliable extraction of the CW and AW is thus essential for characterizing the dominant periodic variability of PM, supporting the interpretation of geophysical excitation processes, and improving PM modelling and prediction (Su et al. 2014; Chen et al. 2023; Nastula et al. 2024).

Existing methods for extracting and reconstructing the CW and AW from PM time series can be reviewed in terms of the assumptions imposed on the target components. Model-based harmonic approaches, commonly implemented through least squares (LS) harmonic fitting, represent the CW and AW using prescribed sinusoidal functions and therefore provide a compact and physically interpretable parameterization when the target frequencies are specified. Their ability to describe the two components is nevertheless constrained by the adopted functional form, particularly when the amplitudes and phases vary with time (Schuh et al. 2001; Hu et al. 2007). Frequency-domain and time-frequency methods, including Fourier transform band pass filtering (FTBPF) and continuous wavelet transform (CWT), relax the fixed harmonic representation by isolating signal energy within selected frequency intervals, but their results depend on passband definition, filter response, window length, and boundary treatment (Popiński and Kosek 1995; Liu et al. 2007; Popiński 2008). Since the CW and AW frequencies are close, these choices directly affect leakage between the two bands and may introduce endpoint distortion in the reconstructed components (RCs). Data-adaptive decomposition methods, such as empirical mode decomposition (EMD) and singular spectrum analysis (SSA), further reduce the need for a prescribed functional model by deriving oscillatory components from the data itself (Lei et al. 2017; Klos et al. 2017; Modiri et al. 2018). However, the extracted components remain dependent on decomposition settings and component-selection criteria; for example, EMD may suffer from mode mixing, whereas the separability of neighboring oscillations in SSA is controlled by the window length and the grouping of RCs (Khazraei and Amiri-Simkooei 2019; Li and Guo 2024). For PM analysis, this difficulty is further complicated by the fact that PMX and PMY are two orthogonal coordinates of the same pole trajectory, whereas many existing procedures analyze them as separate real-valued series (Jin et al. 2021). Such component-wise processing may lead to inconsistent identification or reconstruction of the CW and AW in the two directions,

thereby affecting the relative amplitude and phase relations required to describe their trajectories in the PM plane. Therefore, CW and AW extraction requires a strategy that can separate two neighboring low-frequency oscillations, preserve their time-dependent amplitude and phase characteristics, and maintain the two-dimensional consistency of PM.

To address these requirements, PMX and PMY are represented as a complex-valued series to preserve their coupled two-dimensional relationship during extraction (Liu et al. 2007; Nastula and Gross 2015). On this basis, we propose CoPeX, a complex-domain method that combines the data-adaptive decomposition of SSA with the frequency selectivity of FTBPF for CW and AW extraction. In CoPeX, complex SSA is first applied to obtain preliminary CW and AW components and their spectral characteristics. The components are then extended at both endpoints to reduce finite record boundary effects and refined by FTBPF using component-specific passbands. To compensate for limited spectral information excluded during filtering, constrained sideband recovery is finally introduced, and the recovered contribution is combined with the FTBPF result to obtain the final CW and AW components.

This paper is organized as follows. Section 2 presents the CoPeX methodology and the synthetic and observed PM datasets. Section 3 evaluates the performance of CoPeX using synthetic data through comparisons of reconstructed waveforms and full-record and edge RMSEs. Section 4 applies CoPeX to the IERS EOP 20 C04 series and analyzes the amplitude variations and time–frequency characteristics of the extracted CW and AW. Section 5 discusses the main results, limitations, and conclusions of this study.

2 Methodology and Data

2.1 CoPeX Method

To preserve the relationship between PMX and PMY during extraction, CoPeX represents them as a single complex-valued time series

$$z(t) = \mathrm{PMX}(t) - i\mathrm{PMY}(t) \tag{1}$$

where $i = \sqrt{-1}$ is the imaginary unit. Under this convention, the CW and AW occupy the positive-frequency branch retained in subsequent processing.

Complex SSA is first applied to $z(t)$. For a series $z_n (n = 1, \cdots, N)$ containing N samples and an embedding window of length L, the trajectory matrix $\mathbf{Z}$ is constructed as

$$\mathbf{Z} = \begin{pmatrix} z_1 & z_2 & \mathrm{L} & z_K \\ z_2 & z_3 & \mathrm{L} & z_{K+1} \\ \mathrm{M} & \mathrm{M} & \mathrm{O} & \mathrm{M} \\ z_L & z_{L+1} & \mathrm{L} & z_N \end{pmatrix}, \quad K = N - L + 1 \tag{2}$$

An 8-year embedding window is adopted to cover the approximately 6.4-year beat period between CW and AW, thereby facilitating their separation (Lambert et al. 2006). Singular value decomposition followed by diagonal averaging yields RCs, which are subsequently combined into preliminary CW and AW signals based on their spectral characteristics within the predefined CW (390–500 days) and AW (330–390 days) period ranges. The dominant spectral peak of each preliminary component is then used to define an adaptive passband within the corresponding prescribed range.

Before FTBPF, the SSA components are extended at both ends using the boundary-extension procedure to reduce endpoint distortion caused by the finite record length. Each extended series z_j^{ext}, with $j \in \{\mathrm{CW}, \mathrm{AW}\}$, is then filtered in the Fourier domain. The resulting filtered components z_j^F are given by

$$z_j^F = F^{-1}\{H_j(f)F[z_j^{ext}]\} \tag{3}$$

where F and F^{-1} denote the discrete Fourier transform and its inverse, and $H_j(f)$ is the band pass response at frequency f.

A constrained sideband correction is finally applied to recover residual spectral content within the prescribed physical band but outside the adaptive passband. The final CoPeX estimate is

$$z_j^{CoPeX} = z_j^F + c_j \tag{4}$$

where c_j denotes the sideband correction and is constrained relative to z_j^F to avoid excessive recovery. For comparison, FTBPF is applied directly to the original complex PM series using fixed bands of 390–500 days for the CW and 330–390 days for the AW.

2.2 Data

Synthetic data

A daily synthetic PM series covering 1 January 1984 to 31 December 2025 was generated as

$$z_{syn}(t) = z_C(t) + z_A(t) + z_T(t) + z_N(t). \tag{5}$$

where z_C, z_A, z_T, and z_N denote the CW, AW, trend, and noise components, respectively. The CW and AW are modeled as amplitude-modulated oscillations to represent their time-varying amplitudes (Gross 2000; Wang et al. 2016):

$$z_C(t) = 200[1 + 0.2\cos(\frac{2\pi t}{10000})]exp(-\frac{t}{60000})\exp(i\frac{2\pi t}{433}), 1 \le t \le 15341 \tag{6}$$

$$z_A(t) = 100[1 + 0.2\cos(\frac{2\pi t}{12500})]exp(\frac{t}{100000})\exp(i\frac{2\pi t}{365}), 1 \le t \le 15341 \tag{7}$$

where t is the daily sample index, with $t = 1$ corresponding to 1 January 1984, and amplitudes are expressed in mas. The CW and AW periods are fixed at 433 and 365 days. The slowly varying trend is defined as

$$\begin{aligned} z_T(t) = &\left(50 + 0.55t / 365.2422 + 0.0090(t / 365.2422)^2\right) \\ &-i\left(295 + 1.35t / 365.2422 + 0.0125(t / 365.2422)^2\right) \end{aligned} \tag{8}$$

The noise component is

$$z_N(t) = \alpha\left[0.5\varepsilon(t) + 0.5\eta_{\mathrm{AR}(1)}(t)\right] \tag{9}$$

where $\varepsilon(t)$ and $\eta_{AR(1)}(t)$ are complex Gaussian white noise and complex first-order autoregressive model (AR(1)) noise, respectively, with the latter generated using $\rho = 0.82$. The scale factor α gives a signal-to-noise ratio (SNR) of 15 dB relative to the combined CW and AW signals. The prescribed z_C and z_A series are retained as the reference signals for the quantitative evaluation. The resulting synthetic PM series and its components are shown in Fig. 1.

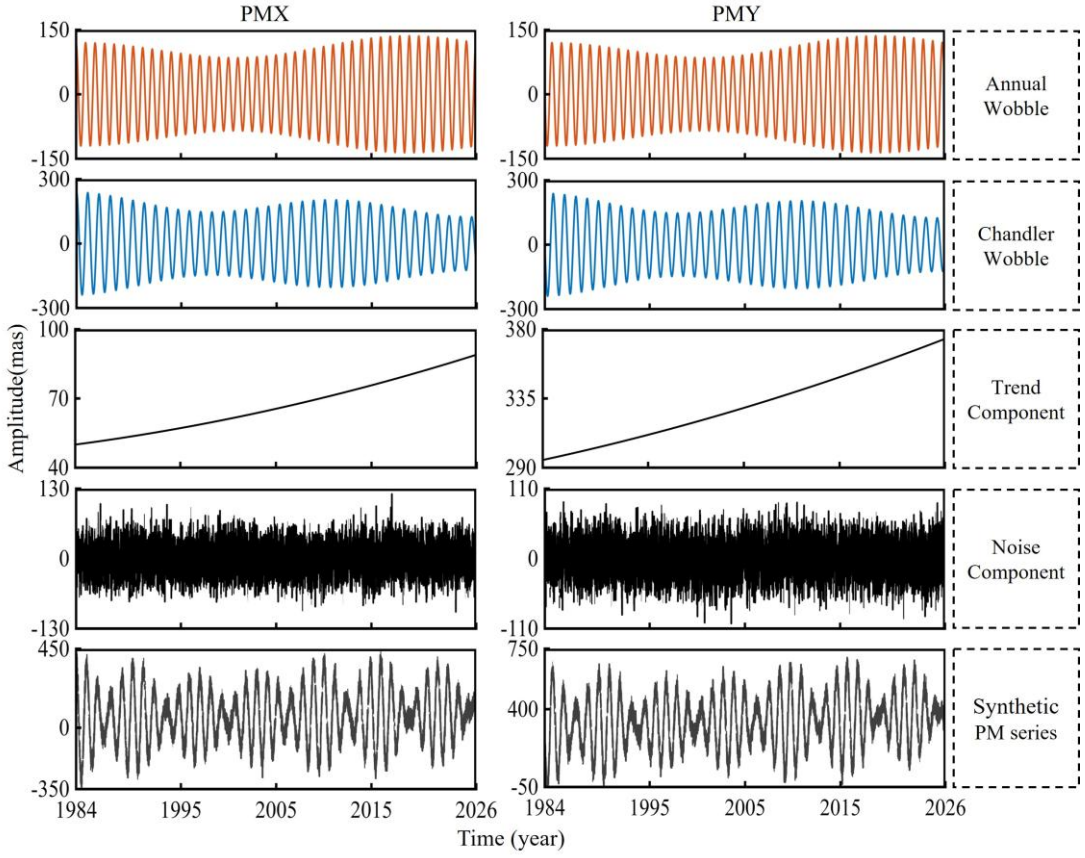


Fig. 1 Synthetic PM series and its prescribed CW, AW, trend, and noise components

Observed data

Daily PM data from 1984 to 2025 are obtained from the IERS EOP 20 C04 series, which combines observations from four space geodetic techniques (Bizouard et al. 2019). The observed and synthetic data have the same temporal coverage and sampling interval. The observed PMX and PMY time series are shown in Fig. 2.

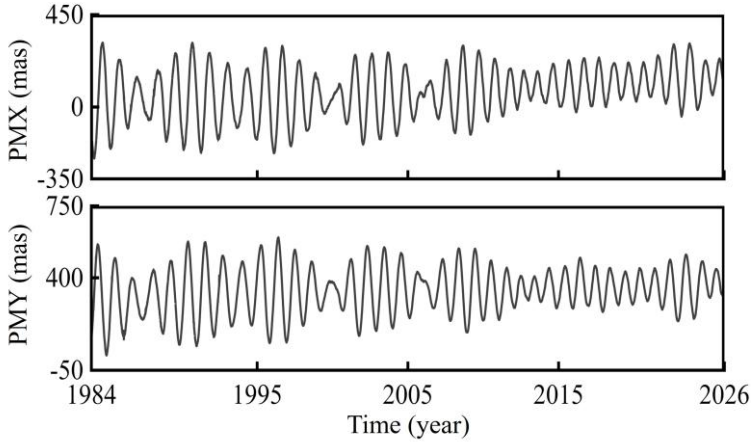


Fig. 2 IERS EOP 20 C04 PM series from 1 January 1984 to 31 December 2025

3 Simulation Validation

The RCs extracted from the synthetic PM series using CoPeX, FTBPF, and SSA are compared in Fig. 3, which shows their amplitude variations, particularly near the endpoints, in both PMX and PMY. FTBPF exhibits a pronounced attenuation in CW amplitude near the right endpoint, whereas no comparable attenuation is observed for SSA and CoPeX. The extraction accuracy of the three methods is further evaluated using RMSEs for the full record and edge regions, as shown in Table 1.

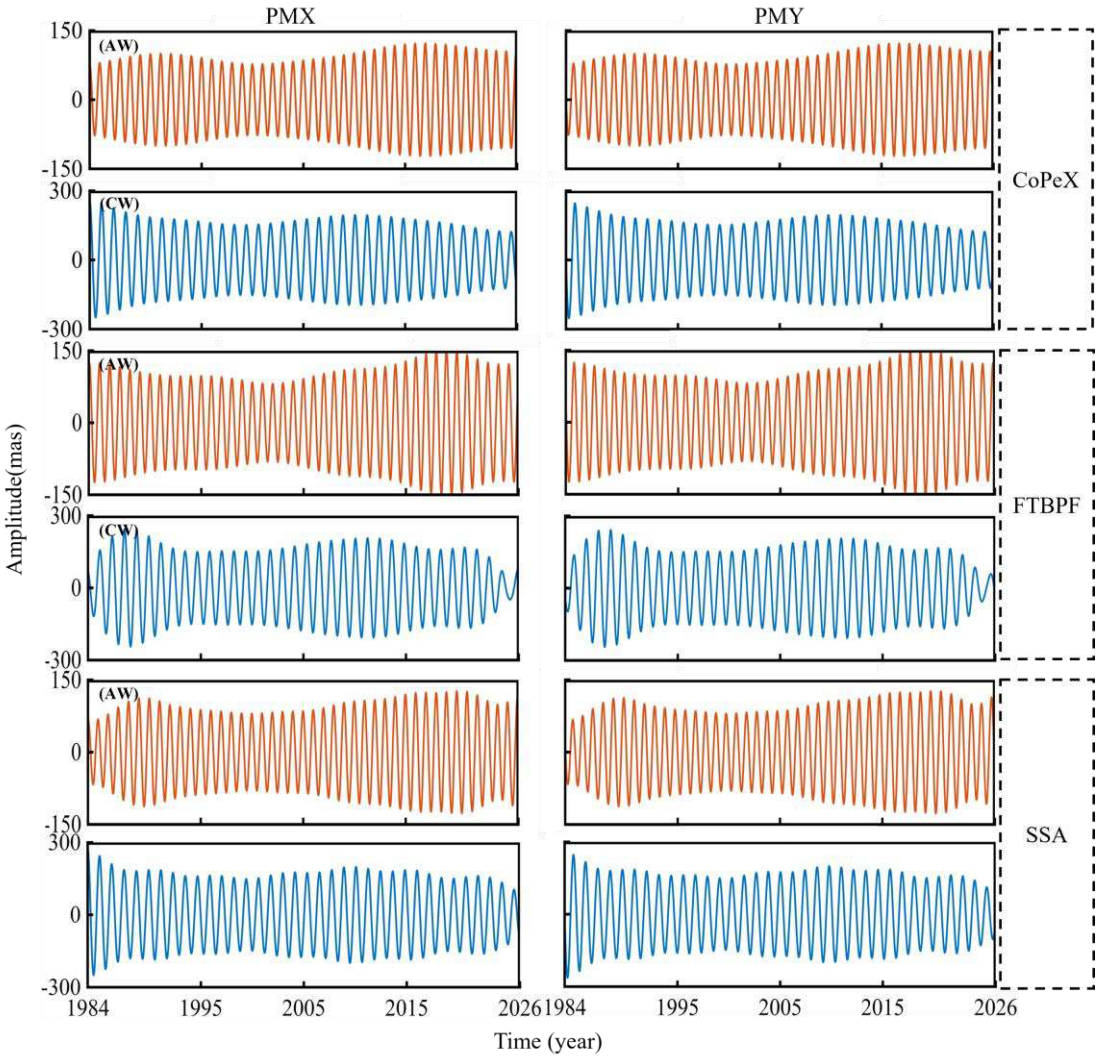


Fig. 3 CW and AW components reconstructed from the synthetic PM series by CoPeX, FTBPF, and SSA

For CW, the full-record RMSE decreases from 19.47 mas with SSA and 37.41 mas with FTBPF to 13.77 mas with CoPeX, corresponding to reductions of 29.30% and 63.20%, respectively (Table 1). The AW RMSE decreases to 18.05 mas, compared with 18.77 mas for SSA and 23.37 mas for FTBPF, giving reductions of 3.84% and 22.76%. These improvements arise from the complementary roles of SSA reconstruction and adaptive frequency selection. The synthetic PM series combines nearby, amplitude-varying CW and AW oscillations with a slowly varying trend and noise. SSA separates the dominant oscillatory structure from this background, while adaptive FTBPF suppresses residual non-target frequencies remaining in the grouped RCs.

The largest boundary errors occur with FTBPF, reaching 113.02 mas for CW and 60.64 mas for AW over the first and last two years. SSA lowers these errors to 34.53 and 43.73 mas, and CoPeX further reduces them to 28.16 and 36.84 mas. The improvement in boundary accuracy is attributable to extending the SSA-reconstructed oscillations before adaptive filtering. The finite PM record has mismatched endpoint amplitudes and phases, which introduce artificial discontinuities under the periodic continuation implicit in Fourier filtering. These discontinuities spread spectral content

across frequencies and distort the reconstructed endpoints. Extending each preliminary component using its endpoint amplitude and phase information maintains the oscillatory connection at the original boundaries, while tapering smooths the outer ends of the extended record. Adaptive FTBPF then suppresses residual non-target frequencies with the original endpoints treated as interior samples, reducing both spectral contamination and truncation-induced distortion.

Table 1 RMSEs of the CW and AW extracted from the synthetic PM series

Method	CW (mas)	AW (mas)	CW edge (mas)	AW edge (mas)
SSA	19.47	18.77	34.53	43.73
FTBPF	37.41	23.37	113.02	60.64
CoPeX	13.77	18.05	28.16	36.84

4 Application to IERS EOP 20 C04

To further evaluate the proposed method using observed data, CoPeX is applied to the IERS EOP 20 C04 PM series. The extracted CW exhibits pronounced long-term amplitude variations. Its annual mean amplitude estimated by CoPeX decreases from 180.85 mas in 1994 to 22.18 mas in 2017, followed by a partial recovery to 35.62 mas in 2025. All three methods capture this evolution in Fig. 4, with differences near the amplitude minimum. The weakening can be interpreted through the combined effects of damping and the relative phases of excitation-driven responses. It may be associated with oceanic and atmospheric angular momentum variations and terrestrial water mass redistribution, with continental air mass changes contributing to atmospheric excitation. These processes may promote partial cancellation among the free wobble and excitation-driven responses, consistent with previous studies (Xu et al. 2024; Jeon et al. 2025).

The AW exhibits more moderate long-term amplitude variations. Its annual mean amplitude estimated by CoPeX increases from 60.94 mas in 1990 to 94.30 mas in 2008 and remains mainly within 81.48–93.40 mas during 2010–2025. This persistent annual oscillation is accompanied by changes in its amplitude envelope, as illustrated in Fig. 4. These AW amplitude variations may be associated with interannual variability in seasonal atmospheric and oceanic angular momentum, together with terrestrial water and ice mass redistribution. Seasonal excitation sustains the annual oscillation, while changes in the strength and relative phase of the individual contributions modify the combined response and its amplitude envelope (Wang et al. 2025b). Multiyear variations in these excitation sources can further modulate the annual response. In particular, episodes of approximately six-year amplitude modulation in annual excitation have been linked primarily to atmospheric angular momentum among the examined climate components (Wang et al. 2025a). Such modulation allows the amplitude envelope to vary over time while the dominant annual periodicity remains persistent. The comparatively stable AW amplitude and its interannual variations obtained here are therefore consistent with sustained seasonal forcing whose strength and composition vary over time.

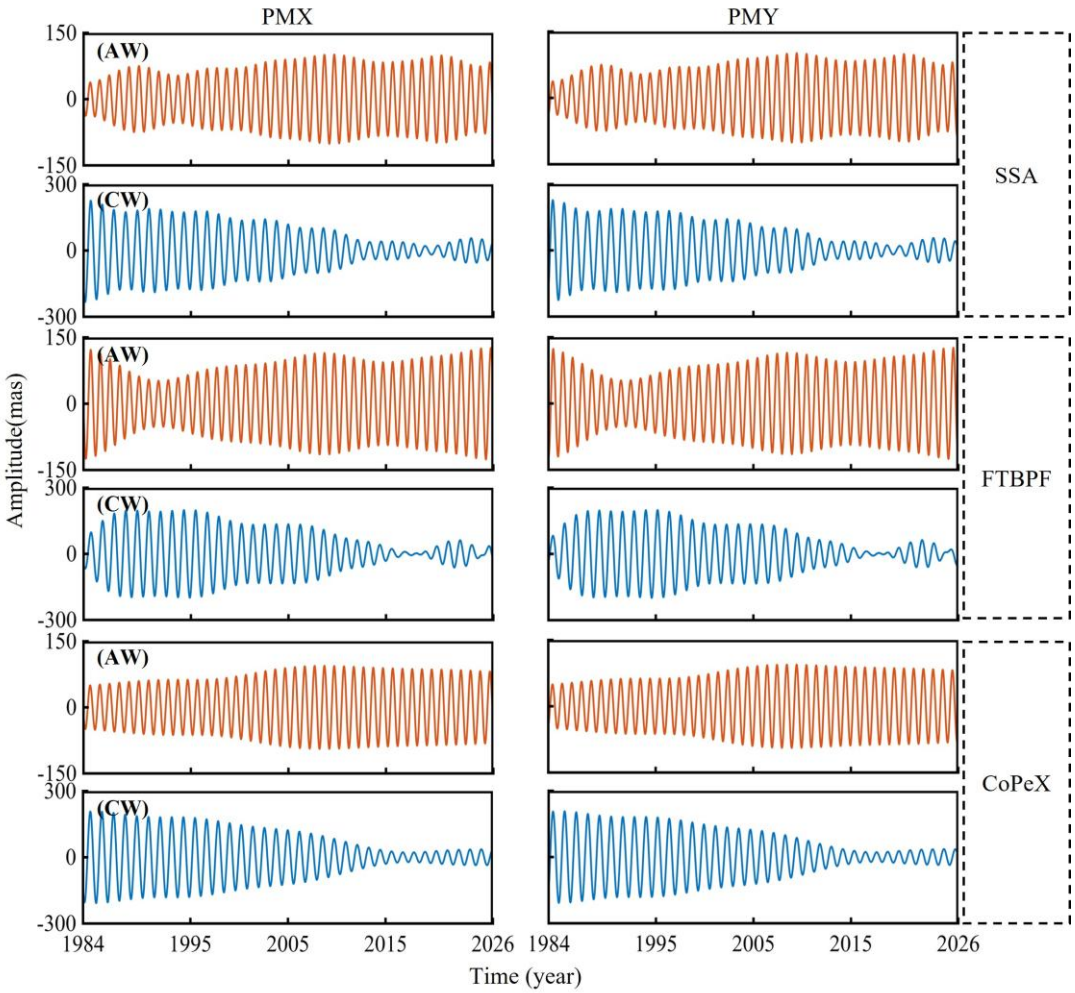


Fig. 4 CW and AW components extracted from the IERS EOP 20 C04 series by SSA, FTBPF, and CoPeX

To relate the amplitude variations in the time domain to their evolving frequency distribution, CWT is applied to the original PM series and the CoPeX reconstructions (Gibert et al. 1998). The original PM spectrum exhibits a broad, connected response region spanning the neighboring CW and AW frequencies, as shown in Fig. 5(a). A strong red patch extends from 1989 to 1992, followed by lower amplitudes in 1993 and 1994. The response strengthens again between 1995 and 1998, forming another red patch before weakening in 1999 and 2000. A weaker orange enhancement appears from 2001 to 2004. After a further low-amplitude interval in 2005 and 2006, another orange patch is visible between 2007 and 2011.

Some troughs are particularly pronounced near the annual frequency, while a discernible response remains in the Chandler frequency region, indicating that trough depth varies with frequency (Iatsenko et al. 2015). From approximately 2013 onwards, the more persistent response lies closer to 1 cpy, with a localized enhancement visible around 2022–2024. The finite frequency width of the Morlet wavelet causes the neighboring CW and AW responses to overlap, with the resultant amplitude determined by their individual response amplitudes and relative phase (Iatsenko et al. 2015). The amplitude patches in the original PM spectrum therefore reflect the changing combined

contribution of CW and AW to PM, with their varying amplitudes and evolving relative phase producing alternating reinforcement and cancellation.

Following separate reconstruction by CoPeX, the CW and AW spectra in Fig. 5(b) and (c) exhibit their principal response bands near 0.84 and 1 cpy, respectively. The principal CW band in Fig. 5(b) remains identifiable throughout the 1990s and 2000s, with its wavelet amplitude varying over time. The AW spectrum in Fig. 5(c) forms a continuous annual band that becomes more pronounced around the turn of the century and remains clearly identifiable through most of the subsequent record, with comparatively moderate amplitude variations. Fig. 5(b) and (c) use the same amplitude scale, allowing direct comparison of their relative response strengths: CW is more prominent in the earlier record, whereas AW is more prominent in the later years. The greater relative prominence of AW in the later period agrees with recent observations showing that PM can be described predominantly by an annual oscillation and long-term drift (Yamaguchi and Furuya 2024). The finite frequency width of the Morlet wavelet also contributes to the weaker responses on either side of each principal band; on the fixed amplitude scale, these surrounding responses become less visible as the principal response weakens (Guilloteau et al. 2021). The comparison thus links the stronger annual-frequency response in the later part of Fig. 5(a) to the greater relative prominence of AW in the CoPeX reconstructions, explaining the evolving frequency distribution of the original PM spectrum in terms of the relative strengths of the two extracted components.

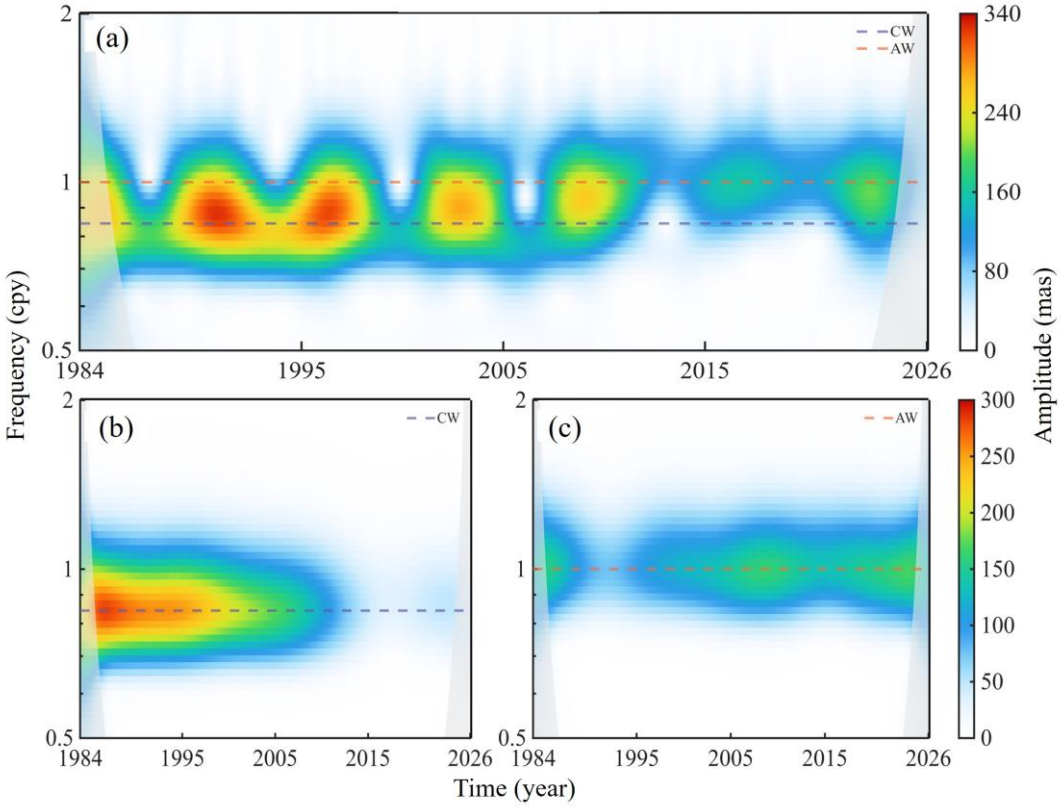


Fig. 5 CWT amplitude spectra of the original PM series (a) and the CW (b) and AW (c) components extracted by CoPeX

5 Discussion and conclusions

CoPeX combines data-adaptive SSA reconstruction with explicit spectral and boundary constraints. Relative to SSA alone, adaptive filtering restricts the frequency content of the preliminary components, while bounded sideband recovery helps retain modulation content excluded by the core passband. CoPeX filters extended SSA components using adaptive bands, whereas FTBPF applies fixed bands directly to the raw PM series. The resulting procedure addresses residual spectral mixing and finite-record boundary sensitivity together, and its net benefit is evaluated by the final reconstruction errors.

In the synthetic experiment, CoPeX gives CW and AW RMSEs of 13.77 and 18.05 mas, corresponding to reductions of 29.30% and 3.84% relative to SSA and 63.20% and 22.76% relative to FTBPF, respectively. Over the first and last two years, the reductions relative to SSA are 18.44% for CW and 15.75% for AW. The adopted configuration therefore reduces the full-record and edge RMSEs for both components, although the full-record gain for AW over SSA remains modest. For the C04 series, the CWT results show retention of the main oscillatory features and their temporal variability.

Since independent CW and AW reference series are unavailable for the C04 data, the absolute extraction accuracy cannot be assessed directly. Future work will explore the use of the extracted components in PM excitation analysis and prediction, and will further assess the applicability of CoPeX to periodic-signal extraction from other geodetic time series, such as GNSS station coordinates and clock-offset series.

Declarations

Funding

This research is funded by the Scientific Research Innovation Capability Support Project for Young Faculty (Grant No. SRICSPYF-ZY2025007), the Basic Science Center Project of the National Natural Science Foundation of China (Grant No. 42388102), the National Natural Science Foundation of China (Grant No. 42574041), the Fundamental and Interdisciplinary Disciplines Breakthrough Plan of the Ministry of Education of China (Grant No. JYB2025XDXM111), and the China Postdoctoral Science Foundation under (Grant No. 2025M770245).

Author contributions

K.Y. developed the initial experimental design. Q.B. conducted the experiments, modified the code, prepared all figures and tables, and wrote the first draft of the manuscript. J.W. provided guidance on the experimental approach. K.Y. and J.W. provided feedback on manuscript revisions. All authors reviewed the manuscript.

Competing interests

No potential conflict of interest was reported by the authors.

Data availability

The IERS EOP 20 C04 polar motion series used in this study is publicly available from the IERS Earth orientation data portal:

https://www.iers.org/IERS/EN/DataProducts/EarthOrientationData/eop.html

Code availability

The MATLAB code implementing CoPeX is provided as supplementary material.

Ethics approval

Ethics, Consent to Participate, and Consent to Publish declarations: not applicable.

References

Bizouard C, Lambert S, Gattano C, et al (2019) The IERS EOP 14C04 solution for Earth orientation parameters consistent with ITRF 2014. Journal of Geodesy 93:621–633. https://doi.org/10.1007/s00190-018-1186-3

Chen W, Chen Y, Ray J, et al (2023) Free decay and excitation of the chandler wobble: self-consistent estimates of the period and quality factor. Journal of Geodesy 97:36. https://doi.org/10.1007/s00190-023-01727-z

Dickey JO, Marcus SL, Johns CM, et al (1993) The oceanic contribution to the Earth's seasonal angular momentum budget. Geophysical Research Letters 20:2953–2956. https://doi.org/10.1029/93GL03186

Gibert D, Holschneider M, Le Mouël J-L (1998) Wavelet analysis of the Chandler wobble. Journal of Geophysical Research: Solid Earth 103:27069–27089. https://doi.org/10.1029/98JB02527

Gross RS (2000) the excitation of the Chandler wobble. Geophysical Research Letters 27:2329–2332. https://doi.org/10.1029/2000GL011450

Guilloteau C, Mamalakis A, Vulis L, et al (2021) Rotated Spectral Principal Component Analysis (rsPCA) for Identifying Dynamical Modes of Variability in Climate Systems. Journal of Climate 34:715–736. https://doi.org/10.1175/JCLI-D-20-0266.1

Höpfner J (2004) Low-Frequency Variations, Chandler and Annual Wobbles of Polar Motion as Observed Over One Century. Surveys in Geophysics 25:1–54. https://doi.org/10.1023/B:GEOP.0000015345.88410.36

Hu X-G, Liu L-T, Ducarme B, et al (2007) Estimation of the pole tide gravimetric factor at the chandler period through wavelet filtering. Geophysical Journal International 169:821–829. https://doi.org/10.1111/j.1365-246X.2007.03330.x

Iatsenko D, McClintock PVE, Stefanovska A (2015) Linear and synchrosqueezed time–frequency representations revisited: Overview, standards of use, resolution, reconstruction, concentration, and algorithms. Digital Signal Processing 42:1–26. https://doi.org/10.1016/j.dsp.2015.03.004

Jeon T, Seo K-W, Youm K, et al (2025) Diminished Chandler Wobble After 2015: Link to Mass Anomalies in 2011. Geophysical Research Letters 52:e2025GL116191. https://doi.org/10.1029/2025GL116191

Jin X, Liu X, Guo J, Shen Y (2021) Analysis and prediction of polar motion using MSSA method. Earth, Planets and Space 73:147. https://doi.org/10.1186/s40623-021-01477-2

Khazraei SM, Amiri-Simkooei AR (2019) On the application of Monte Carlo singular

spectrum analysis to GPS position time series. Journal of Geodesy 93:1401–1418. https://doi.org/10.1007/s00190-019-01253-x

Kiani Shahvandi M, Adhikari S, Dumberry M, et al (2024) Contributions of core, mantle and climatological processes to Earth's polar motion. Nature Geoscience 17:705–710. https://doi.org/10.1038/s41561-024-01478-2

Klos A, Bos MS, Bogusz J (2017) Detecting time-varying seasonal signal in GPS position time series with different noise levels. GPS Solutions 22:21. https://doi.org/10.1007/s10291-017-0686-6

Lambert SB, Bizouard C, Dehant V (2006) Rapid variations in polar motion during the 2005–2006 winter season. Geophysical Research Letters 33:L13303. https://doi.org/10.1029/2006GL026422

Lei Y, Cai H, Zhao D (2017) Improvement of the prediction accuracy of polar motion using empirical mode decomposition. Geodesy and Geodynamics 8:141–146. https://doi.org/10.1016/j.geog.2016.09.007

Li W, Guo J (2024) Extraction of periodic signals in Global Navigation Satellite System (GNSS) vertical coordinate time series using the adaptive ensemble empirical modal decomposition method. Nonlinear Processes in Geophysics 31:99–113. https://doi.org/10.5194/npg-31-99-2024

Li Z, Yu K, Shi K, et al (2026) A New Short-Term Polar Motion Prediction Method Based on Combination of LS Model with Time-Varying Characteristics and Arima Model. Journal of Earth Science 37:870–881. https://doi.org/10.1007/s12583-025-0319-x

Liu L, Hsu H, Grafarend EW (2007) Normal Morlet wavelet transform and its application to the Earth's polar motion. Journal of Geophysical Research: Solid Earth 112:B08401. https://doi.org/10.1029/2006JB004895

Modiri S, Belda S, Heinkelmann R, et al (2018) Polar motion prediction using the combination of SSA and Copula-based analysis. Earth, Planets and Space 70:115. https://doi.org/10.1186/s40623-018-0888-3

Nastula J, Gross R (2015) Chandler wobble parameters from SLR and GRACE. Journal of Geophysical Research: Solid Earth 120:4474–4483. https://doi.org/10.1002/2014JB011825

Nastula J, Śliwińska-Bronowicz J, Wińska M, Kur T (2024) Analysis of combined series of hydrological angular momentum developed based on climate models. Frontiers in Earth Science Volume 12:1369106 https://doi.org/10.3389/feart.2024.1369106

Popiński W (2008) Insight into the Fourier Transform Band Pass Filtering Technique. Artificial Satellites 43:129–141. https://doi.org/10.2478/v10018-009-0012-9

Popiński W, Kosek W (1995) The Fourier transform band pass filter and its application for polar motion analysis. Artificial Satellites 30(1):9–25

Rekier J, Chao BF, Chen J, et al (2022) Earth's Rotation: Observations and Relation to Deep Interior. Surveys in Geophysics 43:149–175. https://doi.org/10.1007/s10712-021-09669-x

Schuh H, Nagel S, Seitz T (2001) Linear drift and periodic variations observed in long time series of polar motion. Journal of Geodesy 74:701–710. https://doi.org/10.1007/s001900000133

Shi Q, Zhou Y, Chen J, Xu X (2025) Recent disappearing and re-excited Earth's Chandler wobble: contributions from GRACE/GFO hydrological and cryospheric mass changes. Journal of Geodesy 99:97. https://doi.org/10.1007/s00190-025-02021-w

Su X, Liu L, Houtse H, Wang G (2014) Long-term polar motion prediction using normal time–frequency transform. Journal of Geodesy 88:145–155. https://doi.org/10.1007/s00190-013-0675-7

Wang G, Liu L, Su X, et al (2016) Variable Chandler and Annual Wobbles in Earth's Polar Motion During 1900–2015. Surveys in Geophysics 37:1075–1093. https://doi.org/10.1007/s10712-016-9384-0

Wang S, Wilson CR, Chen J, et al (2025a) Variability of annual polar motion and its relationship to the Chandler wobble. Proceedings of the National Academy of Sciences 122:e2520272122. https://doi.org/10.1073/pnas.2520272122

Wang S, Wilson CR, Chen J, Seo K-W (2025b) Annual polar motion and its variability. Journal of Geodesy 99:57. https://doi.org/10.1007/s00190-025-01982-2

Xu X-Q, Fang M, Zhou Y-H, Liao X-H (2024) Continental and oceanic AAM contributions to Chandler Wobble with the amplitude attenuation from 2012 to 2022. Journal of Geodesy 98:59. https://doi.org/10.1007/s00190-024-01872-z

Yamaguchi R, Furuya M (2024) Can we explain the post-2015 absence of the Chandler wobble? Earth, Planets and Space 76:1. https://doi.org/10.1186/s40623-023-01944-y

Yu K, Wang X, Li Z, et al (2025) Near real-time LOD prediction using ConvLSTM model through integrating IGS rapid LOD and effective angular momentum. Geo-spatial Information Science 28:3196–3210. https://doi.org/10.1080/10095020.2025.2471432

Supplementary Files

This is a list of supplementary files associated with this preprint. Click to download.

- code.zip